$11^{th}$ International Conference on Fracture Mechanics of Concrete and Concrete Structures
FraMCoS-11
J. M. Chandra Kishen, A. Ramaswamy, S. Ray and R. Vidyasagar (Eds)
https://doi.org/10.21012/FC11.092365

# STUDY OF DAMAGE MECHANISMS IN ULTRA HIGH PERFORMANCE CONCRETE USING ACOUSTIC EMISSION TECHNIQUE

**MD ADIL AHMED*, SUDAKSHINA DUTTA†**

*Department of Civil Engineering, Indian Institute of Technology
Roorkee, India
e-mail: ma_ahmed@ce.iitr.ac.in

†Department of Civil Engineering, Indian Institute of Technology
Roorkee, India
e-mail: sudakshina@ce.iitr.ac.in

**Key words:** Ultra high performance concrete, Interface, Fiber bridging, Acoustic Emission, AE Entropy

**Abstract.** This paper deals with the study of fiber-matrix bond properties in ultra-high performance concrete (UHPC) by performing pullout tests on straight single steel fibers of varying aspect ratios, embedded partially in the concrete matrix. The interface between the fiber and the matrix plays a major role in enhancing the toughness of the material. It is the weakest link in the composite from where damage initiates. Hence, it is crucial to study the interface bond properties, and the most direct method to study them is the single fiber pullout test. The pullout load vs. fiber slip is recorded to analyze the pullout behavior of the fiber. The failure mechanism of fiber embedded in matrix takes place in different stages. To identify these stages, acoustic emission (AE) technique is implemented. An AE parameter based on Shannon's entropy is used. The AE entropy, being independent of threshold, in addition to AE event amplitude and energy are recorded. The study establishes a correlation between the AE signal parameters and different stages of damage in the fiber pullout process. It is observed that the AE entropy parameter differentiated the damage stages in the fiber pullout process more efficiently than the other AE parameters.

## 1 INTRODUCTION

Ultra High Performance concrete (UHPC) is a special type of concrete with higher compressive strength and better ductility compared to conventional concrete. It was first developed by Richard et. al [1] and was called Reactive Powder concrete (RPC). It has a dense microstructure due to incorporation of ultrafine particles. A high range water reducers are used to compensate for its low water to binder ratio [2]. The incorporation of fibers enhances its tensile strength, fracture toughness, energy absorption and ductility. Utilization of supplementary cementitious materials like fly ash, silica fume, ground granulated blast-furnace slag (GGBS), etc., as partial replacement of ordinary portland cement (OPC) leads to a reduction in the emission of greenhouse gases, thereby making it a more eco-friendly alternative.

The usage of fiber reinforced composites has increased in recent years due to their high strength to weight ratio, more durability and longer service life compared to traditional materials. Both the fiber and the matrix in fiber reinforced composites retain their original physical and chemical properties, yet they impart mechanical properties to the composite which

cannot be provided by the components acting alone. The interface between the fiber and the matrix plays a major role in enhancing the strength, toughness and fracture resistance of the composite. However, it also forms the weakest link in the composite where crack initiation takes place. Thus, it is crucial to understand the fiber-matrix interface behavior.

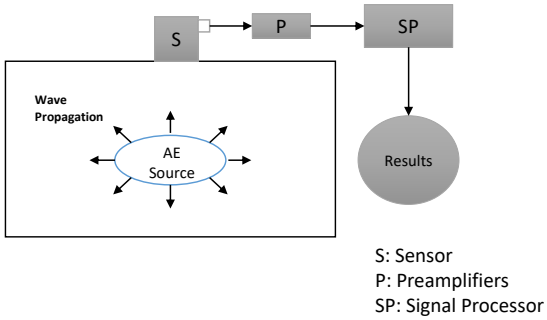


**Figure 1:** AE detection principle.

Fiber pullout test is a direct method to study the fiber-matrix interface bond properties. Tuyan et al. [3] studied the effect of embedment length and aspect ratio on the single fiber pullout tests on the slurry infiltrated fiber concrete (SIFCON) matrix. It was observed that the peak pullout load and the toughness increased with the increase in the embedment length. A linear relationship existed between the toughness and embedment length for straight fibers. With the increase in aspect ratio, the peak pullout load decreased for equal fiber lengths. Breitenbucher et al. [4] studied the bond mechanism of steel fibers in high and normal-strength concrete by investigating their pullout behavior. There was an appreciable drop in the pullout force after complete debonding for straight steel fibers, beyond which only frictional forces acted between the fiber-matrix interface. A larger pullout force has been observed for fibers embedded in high-strength concrete than normal-strength concrete. Wu et al. [5] investigated the interfacial bond property for different types of steel fibers in UHPC matrix having silica fume content of 15%, or 20% by mass of binder at different curing ages. On conducting the fiber pullout test, it was observed that for straight fibers, the peak load was followed by complete debonding and pulling out of the fiber from the matrix. Yoo et al. [6] studied the effect of embedment length of straight and half hooked steel fiber in a UHPC matrix when subjected to a pullout load. There was a linear increment in the pullout energy of the straight fiber with the increase in its embedment length.

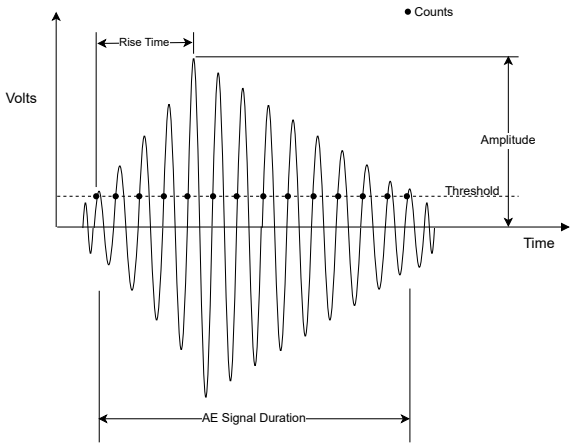


**Figure 2:** AE parameters.

### 1.1 Fracture study using acoustic emission technique

Acoustic emission (AE) is defined as a process in which due to the deformation or cracking in a solid, the stored strain energy is released thereby generating elastic waves. In concrete the major source of acoustic emissions are from the cracking of matrix and the friction between the separated surfaces. If fibers are present in the concrete, its pullout or fracture leads to the generation of AE waves. Figure 1 depicts the AE detection principle. Mechanical waves generated from the acoustic emission sources are captured by the sensors that are fixed on the sample surface. These waves are amplified by a preamplifier, which then transmits it to the AE signal processor where it is processed to extract relevant information [7]. The various parameters that comprises the AE signal are counts, amplitude, rise time, duration, etc., as shown in

Figure 2

### 1.1.1 AE entropy - An alternative to other AE parameters

A reliable process to assess the various damage stages during the pullout of fiber from UHPC matrix is scarce. One of the ways to measure the damage is to record the disorder generated in this process. These disorder are in the form of breaking of the bond between the fiber and the matrix, and friction generated due to sliding of fiber against the matrix followed by damage of the matrix tunnel. Different AE parameters such as - AE signal amplitude, AE count, counts to peak, energy, rise time, duration, etc., can be used to identify these mechanisms. Santo et al. [8] studied the influence of threshold on AE count, rise time, duration, energy, amplitude, and entropy, by generating elastic waves in the metal plate by Pencil Lead Break test. It was observed that except for AE entropy and amplitude, all the other parameters decreased with the increase in threshold value. The peak amplitude, though independent of threshold, did not contain the information from the discrete voltage values of the waveform. Thus, it could not predict the nature of the waveform. However, this was not the case with AE entropy, which was obtained from the probability distribution of the discrete voltage values of a waveform, including those which were even below the threshold level. Moreover, it was also observed that AE entropy was independent of Hit Definition Time (HDT) whereas other parameters such as amplitude, count, duration, and energy were dependent on the HDT settings. Burud et al. [9] used wavelet entropy as a damage index to identify the multi-mechanistic fracture process in plain concrete under flexural loading. A high variance of the wavelet entropy distribution implied the existence of the multi-mechanistic and multi-source fracture process. The cumulative AE entropy derived from AE counts was used to identify the damage evolution in composite. The cumulative entropy distinguished the three stages of the damage evolution better than the cumulative AE counts [10]. Amiri et al. [11] utilized the Shannon entropy to determine the initiation and growth of fatigue cracks in aluminum alloys and observed that both the evolution of AE entropy and AE hit count correlated well. Karimian et al. [12] utilized the information entropy of AE signals to detect initiation of fatigue cracks in aluminum alloy. It was observed that before the formation of macrocracks, the information entropy reaches its minimum value and the cumulative information entropy increases rapidly preceding macrocrack propagation. It was also seen that the cumulative entropy was not significantly affected by the location of the measurement. Kahirdeh et al. [13] used information entropy as an AE parameter to assess the degradation of titanium alloy when subjected to fatigue cracking testing. He concluded that at the time of fatigue failure the entropy reached its maximum value for both the cases irrespective of the loading condition or the path of the fatigue crack growth.

Studies on identifying the fiber pullout damage stages in UHPC matrix using AE entropy is sparse. Therefore, the objective of this investigation is to study the efficiency of AE entropy based on Shannon's entropy to identify the different damage stages during a fiber pullout process with varying embedment lengths and aspect ratios.

## 2 METHODOLOGY

Each AE waveform generated during the fiber pullout process will have a unique disorderness. The measure of this disorderness could be used to identify the various stages of fiber pullout process. The discrete voltage value of a waveform provides its probability distribution [8], which can be quantified as information entropy.

The information entropy was first introduced by Shannon [14] in 1948. For a given random sequence $x_1, x_2, x_3, ...x_n$, the Shannon's entropy is given by:

$$H = -c \sum_{i=1}^{n} p(x_i) * log(p(x_i)) \qquad (1)$$

**Table 1:** Mix Proportion

| Unit Weight (kg/m$^3$) | | | | | | |
|---|---|---|---|---|---|---|
| Cement | Silica Fume | GGBS | Quartz Powder | Sand | Water | Superplasticizer |
| 716.8 | 102.4 | 204.8 | 77.0 | 925.0 | 201.4 | 20.0 |

**Table 2:** Detail of Steel Fiber dimension

| Fiber Type | Fiber Diameter (mm) | Fiber Length (mm) | Aspect Ratio |
|---|---|---|---|
| Straight Steel Fiber (S26) | 1 | 26 | 26 |
| Straight Steel Fiber (S74) | 0.7 | 52 | 74 |

Where, H is the non-negative Shannon's entropy. For a given random sequence $x_i$, $p(x_i)$ is its associated probability mass. The entropy is measured in bits if c, an arbitrary positive constant, equals 1/log(2) making the logarithm base as 2. Keeping the measurement unit in bits enables the representation of average amount of information or uncertainty in binary coding, which is the most efficient way to represent information in a digital system.

## 3 EXPERIMENTAL PROGRAM

### 3.1 Materials and specimen preparation

A summary of the mix proportion for UHPC matrix used in this study has been given in Table 1. Ordinary Portland Cement of Grade 43 forms a major portion of the mixture. The water to binder ratio is kept at 0.2. Silica fume or micro silica, and GGBS, are used as 10% and 20% partial replacement of cement, respectively. To decrease the porosity of the matrix, quartz powder is used. Fine aggregates of size less than 4.75 mm and Polycarboxylate based superplasticizer are also used in the mixture. To improve the homogeneity of the mix, coarse aggregate are not included in the mixture. The cube compressive strength for UHPC matrix was equal to 100 MPa.

Straight steel fibers are used for the fiber pullout test, details of which are given in Table 2. In order to study the pullout behavior and to identify the different damage stages using AE paramaters, straight steel fibers of embedment lengths of 30%, 40%, and 50% of the total fiber length and aspect ratio of 26 (S26) and 74 (S74) are used.

### 3.2 Test Setup

**Figure 3:** Fiber pullout and AE monitoring test.

The fiber pullout tests is performed in a benchtop universal testing machine of 25 kN capacity. The specimen is fixed at the base plate using metallic bolts as shown in Figure 3. The free end of the fiber is clamped tightly using screws so as to avoid slippage of fiber during

testing when it is being pulled out at a rate of 0.8 mm/min.

For AE monitoring, four piezoelectric sensors (MISTRAS R6I) with integrated preamplifiers (40 dB gain) are used as shown in Figure 3. To eliminate the background noise, the threshold is set at 35 dB.

## 4 RESULTS AND DISCUSSIONS

The resistance to pullout forces on straight fiber is provided by the chemical adhesion followed by the frictional force between the fiber and the matrix. The fiber pullout stages include the debonding stage (o-a-b) (refer Figure 5) due to cracking in the interfacial transtition zone along the length of the fiber. A rapid increase in the pullout load is observed in this region, followed by a sharp decline at (b) where complete debonding has taken place. It is followed by the frictional pullout stage (b-c). Only kinetic friction exists between the fiber and the matrix after complete debonding stage. With the increase in fiber slip the pullout load decreases in this region (b-c).

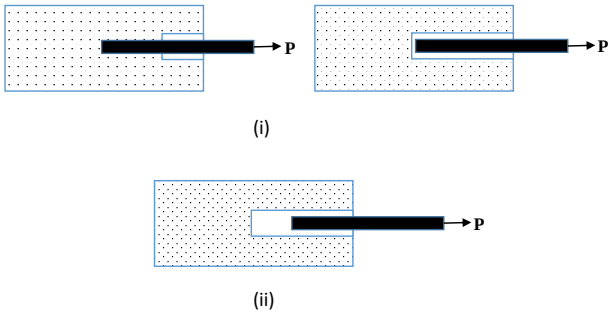


**Figure 4:** Pullout behavior of straight steel fiber in (i) Debonding Stage (o-a-b), (ii) Frictional Stage (a-b).

The pullout mechanisms of a straight fiber is depicted in Figure 4. The average pullout load vs. slip curve depicting the different damage stages for 50% fiber embedment length is shown in Figure 5. Similar behavior is also observed for other fiber embedment lengths which is discussed in the following sections along with the identification of the damage stages using different AE parameters.

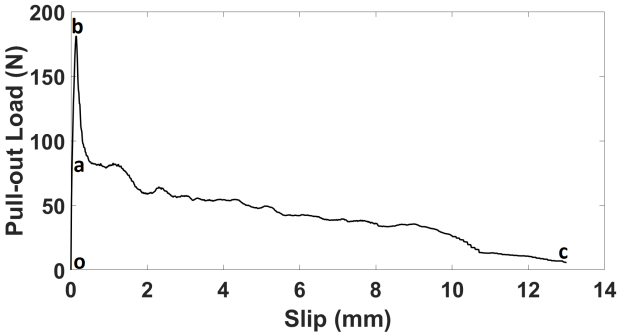


**Figure 5:** Pullout load-slip curve for straight fiber with different damage stages.

### 4.1 Effect of embedment length

To study the effect of embedment length on the pullout behavior of straight end steel fiber, three different percentages of embedment length, i.e., 30%, 40%, and 50%, are considered. The average load-slip behavior for the three different embedment lengths is shown in Figure 6. Table 3 summarises the peak load and the maximum slip values. The average maximum pullout load increases by 75% and 37% for both 50% and 40% fiber embedment lengths, respectively, as compared to 30% embedded length. Similarly, an increase in the average slip values for 50% and 40% fiber embedment lengths are around 69% and 43%, respectively, when compared with the 30% fiber embedment length. With the increase in the embedment lengths of the fiber, a larger portion of fiber comes in contact with the concrete matrix which increases the fiber-matrix bonding area. The increased bond area enhances the load transfer between the fiber and the surrounding concrete matrix which results in a higher peak load during the pullout test. Moreover, with the increase in the embedment lengths of the fiber the frictional resistance along the fiber matrix interface also increases. A higher external load is now needed to overcome the frictional force in order to pull the fiber out of the matrix, leading to an increase in the peak load and slip value.

**Table 3:** Straight fiber pullout test results

| % Fiber Embedded | Avg. Peak Load (N) | Avg. Max Slip (mm) |
|---|---|---|
| 50 | 181 | 13 |
| 40 | 141 | 11 |
| 30 | 103 | 7.7 |

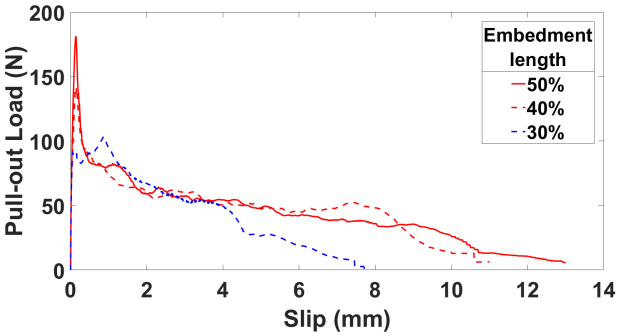


**Figure 6:** Pullout load-slip curve for straight fiber of 50%, 40%, and 30% embedment length.

### 4.2 AE Parameter observations

*(a) Efficiency of AE Entropy against other AE parameters:* Figure 7(a) depicts the evolution of AE entropy throughout the different stages of the straight fiber pullout test for 50% embedment length. Initially when the bond between the fiber and the concrete matrix commences to break with an increase in the pullout load, large amount of elastic waves are generated. A large number of AE entropy, corresponding to these AE signals, clustered very closely to each other are obtained. The magnitude of entropy depends on the disorderness associated with each waveform. In the debonding process, AE waves with highly dispersed waveforms in terms of amplitude are released which forms AE entropy of a higher magnitude till the peak load. Once the peak load is reached, the fiber then begins to slide relative to the concrete matrix. The frictional force which now acts at the interface between the fiber and matrix resists this relative motion, and results in generation of elastic waves. It is observed that the number of elastic waves, and in turn the AE entropy, generated during the frictional stage is relatively low compared to the debonding stage. This can be attributed to a much more steady pullout process of fiber in the frictional stage as compared to the abrupt debonding process. Further, it is also observed that the magnitude of entropies generated during the frictional stage of the fiber pullout process are comparatively lower than the debonding stage. It occurred due to a more uniform distribution of stress and hence a fewer localized stress concentration along the fiber-matrix interface during the frictional stage as compared to the debonding stage. The AE waves generated during this stage has a lower degree of disorderness and a lower peak amplitude as compared to the waves generated in the debonding stage. All these factors led to the generation of lower magnitude AE entropy that are less concentrated in number as compared to the entropy in the debonding stage. Similar observations are also made for straight steel fibers whose 40% and 30% of the total length of the fiber is embedded inside the concrete matrix as shown in Figure 8(a) and 9(a), respectively.

Compared to AE entropy, the number of AE events amplitude recorded during the entire fiber pullout process, as shown in Figures 7(b), 8 (b), and 9(b) for 50%, 40%, and 30% fiber embedment lengths, respectively, are very less. An event is detected when a minimum of three hits are detected simultaneously for a 2D planar analysis. During the straight fiber pullout process, few AE event amplitudes are recorded in the debonding stage of the fiber pullout test. In the frictional stage, the AE events amplitude recorded are negligible due to a relatively low release of energy during this process which might have been filtered out due to the threshold settings. Similarly, the absolute energy corresponding to the AE events have been shown in Figures 7(c), 8 (c), and 9(c) for 50%, 40%, and 30% fiber embedment lengths, respectively. Besides being threshold dependent, the magnitude of absolute energy for all the three fiber embedment lengths are not uniform in the different damage stages. In the debonding stage itself, significant differences can be seen between the maximum values of the absolute energy for different fiber embedment lengths that are not observed in case of AE entropy. Hence, due to

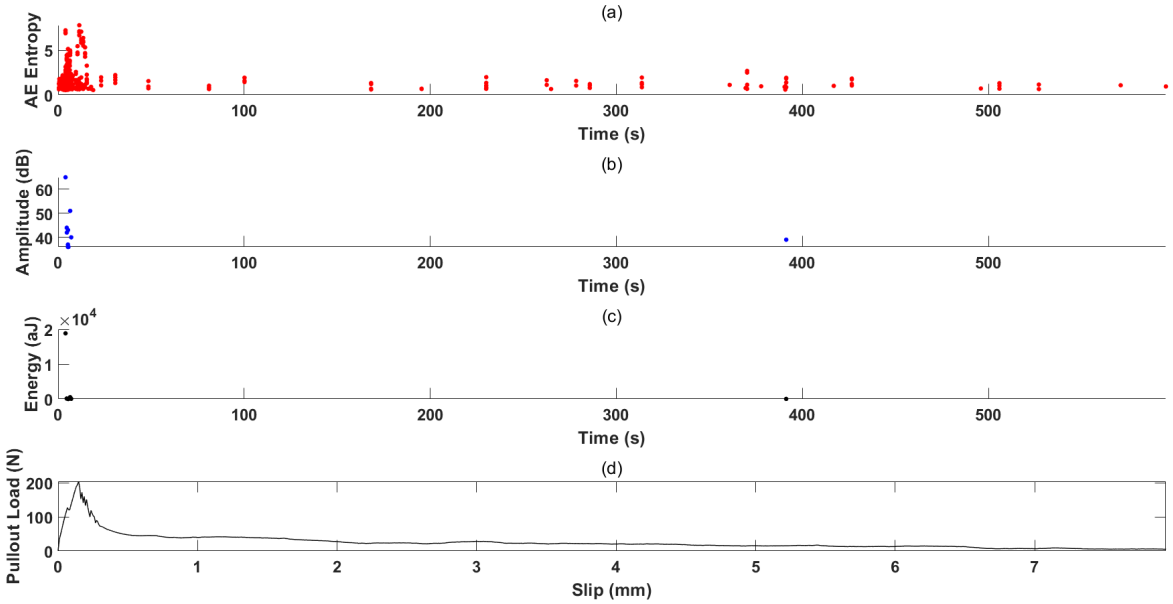


**Figure 7:** AE Parameters for 50% fiber embedded length.

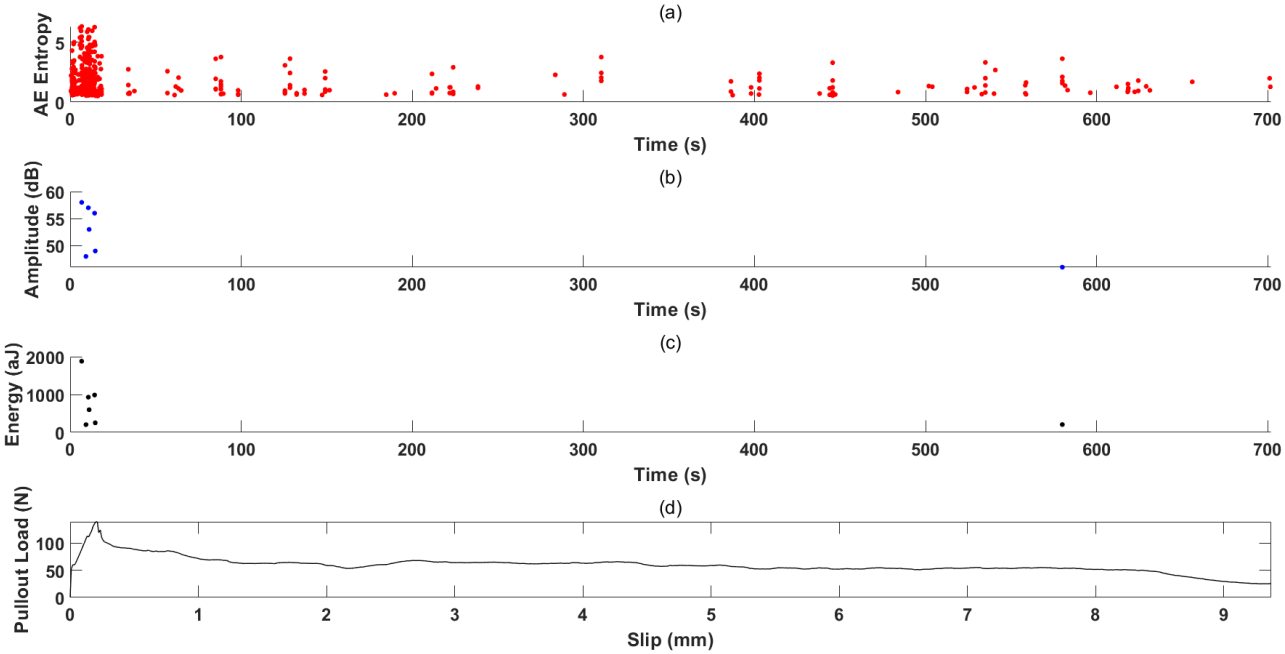


**Figure 8:** AE Parameters for 40% fiber embedded length.

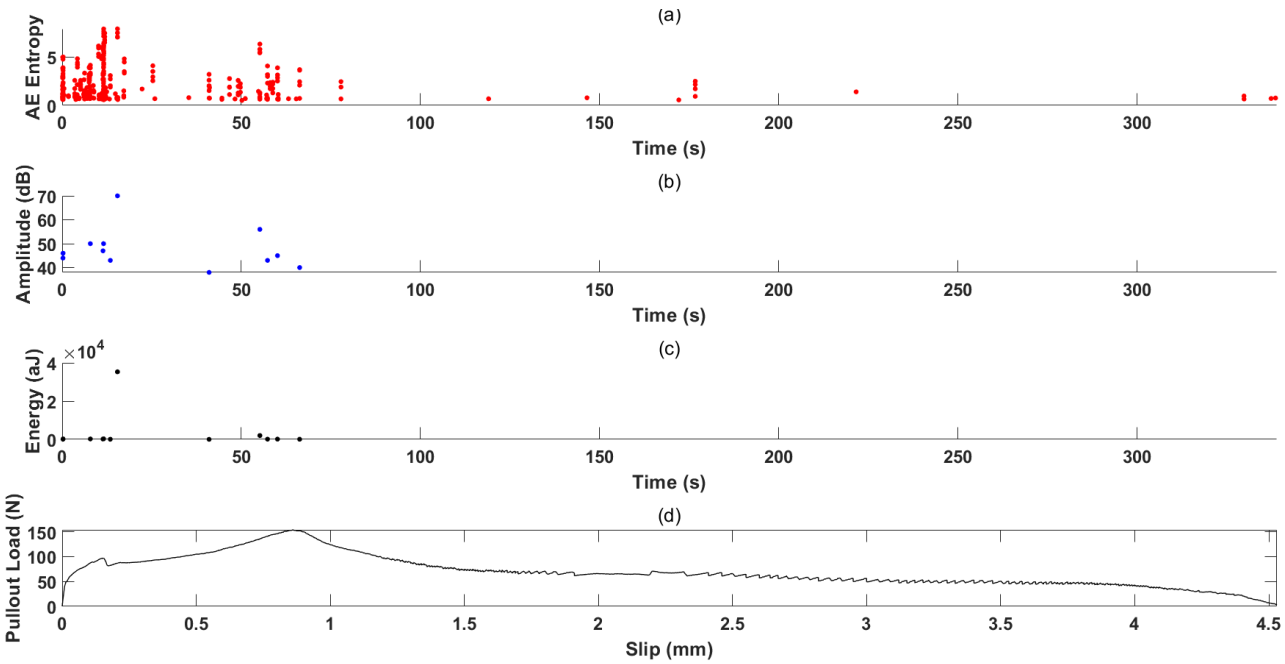


**Figure 9:** AE Parameters for 30% fiber embedded length.

these observations, the AE event amplitude and absolute energy parameter proved to be less effective compared to the AE entropy in identification of the damage stages.

*(b) Cumulative AE Parameter:* Figure 10, depicts the comparison between the evolution of cumulative entropy, with different fiber embedment lengths subjected to the pullout load. During AE monitoring, both the cumulative amplitude and cumulative energy have been used for damage assessment in the past. It gives an insight into the damage accumulation and energy released within a material over time. Hence, the cumulative entropy is used in this study to investigate its usage in determining the fiber pullout damage stages. The variation in cumulative entropy is found to be similar for the three fiber embedment lengths. At the beginning of the pullout process, the cumulative entropy rapidly increases signifying the initial debonding stage. With progression of the debonding zone, the entropy further increases with a slight decrease in the slope. Post peak load, the slope of the cumulative entropy curve decreases considerably, signifying a decrease in the generation of AE entropy. This region can be identified as the frictional stage, as the AE signals generated are comparatively fewer in numbers and magnitude. Thus, the cumulative AE entropy could satisfactorily identify the different damage stages during the straight fiber pullout process.

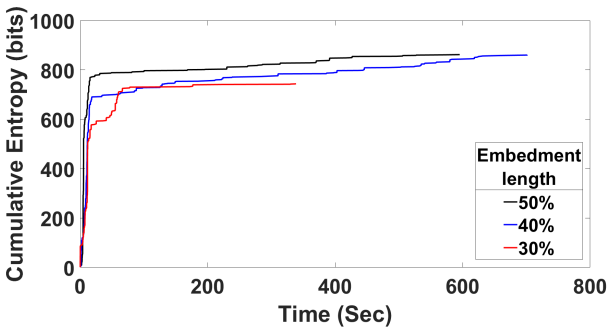


**Figure 10:** Cumulative Entropy for straight fiber of 50%, 40%, and 30% embedment length.

Figures 11 and 12 depict the variation of event cumulative amplitude and absolute energy, respectively, with time during the fiber pullout test for all the three fiber embedment lengths. Unlike cumulative entropy, these curves do not show a similar trend. Even though the debonding stage could be identified with the rapid increase in the cumulative values, the frictional stage was not depicted for the 30%

fiber embedment length due to no events being recorded in that stage. Similarly, due to lack of detection of events in the frictional stage of 40%, and 50% embedded fibers, the cumulative curve for the entire pullout duration was not obtained. Moreover, the 30% fiber embedded length showed the highest release of cumulative absolute energy and cumulative amplitude followed by 50% and then by 40% fiber embedded length. Such discrepancies are not observed for cumulative entropy.

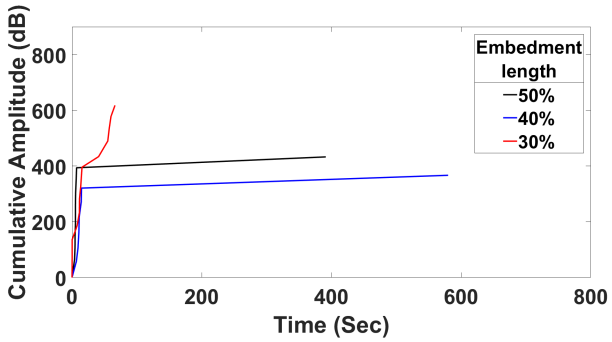


**Figure 11:** Cumulative amplitude for straight fiber of 50%, 40%, and 30% embedment length.

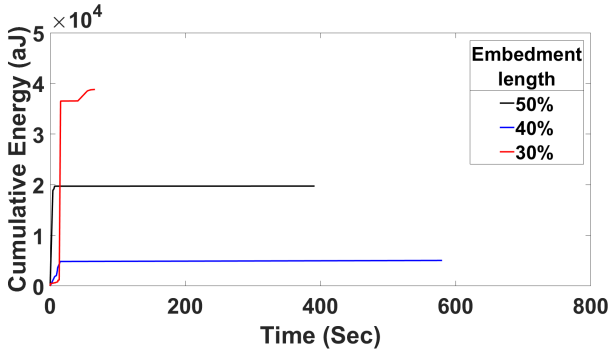


**Figure 12:** Cumulative energy for straight fiber of 50%, 40%, and 30% embedment length.

### 4.3 Effect of aspect ratio

Aspect Ratio of a fiber is defined by the ratio of its length to its diameter. The average pullout load vs. slip behavior for straight steel fiber with aspect ratios 26 (S26) and 74 (S74) is shown in Figure 13. While there is not much difference in the peak load recorded, the post peak behavior varied significantly. Fiber with higher aspect ratio has more surface area in contact with the concrete matrix which enables them to absorb more amount of energy to go through the stages of debonding and friction, between the fiber-matrix interface, during its pullout process. This increases the toughness as depicted by the amount of pullout energy needed by the higher aspect ratio fiber (S74) to be nearly 4 times than the lower one (S26). It is also observed that the maximum slip for fiber - S74 was double than that of the maximum slip for fiber - S26 as shown in Table 4. Steel fiber with higher aspect ratio has a longer length relative to its diameter. The longer fiber embedded inside the matrix provides a greater bonding length along the fiber-matrix interface. This allows for more efficient transfer of load between the fiber and the matrix. Moreover, the distribution of tensile stress becomes more effective and uniform with the increase in the embedded length, thereby causing a more gradual pullout process.

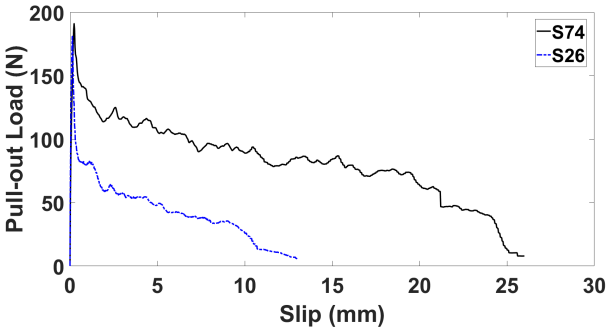


**Figure 13:** Pullout Behavior comparison between straight fiber of aspect ratio 26 and 74.

**Table 4:** Effect of aspect ratio on the pullout behavior of straight steel fiber

| Fiber Code | Aspect Ratio | Avg. Peak Load (N) | Avg. Max Slip (mm) | Pullout Energy (N.mm) |
|---|---|---|---|---|
| S26 | 26 | 181 | 13 | 563 |
| S74 | 74 | 191 | 26 | 2130 |

Figure 14 depicts the variation of cumulative AE entropy with respect to the aspect ratio. Both the curves followed a similar trend. A rapid increase in the cumulative entropy initially depicts the debonding stage which is followed by a decrease in its rate, and the slope

becoming almost parallel to the time axis in the frictional stage. With the increase in the aspect ratio, the contact area between the fiber and matrix increases leading to more area being subjected to debonding and frictional resisting forces. This leads to the release of more AE signals from which the AE entropies are derived.

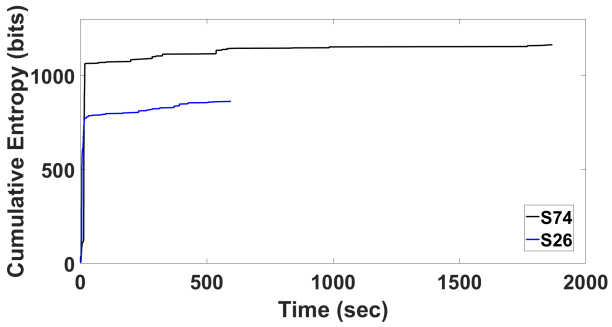


**Figure 14:** Cumulative AE entropy comparison between straight fiber of aspect ratio 26 and 74.

## 5 CONCLUSION

Fiber-matrix bond properties in UHPC have been studied by performing single fiber pullout test on straight steel fiber. It is observed that the increase in the embedment length and the aspect ratio of the fiber increases the peak pullout load, maximum slip, and pullout energy. In order to identify the different damage stages, AE entropy based on Shannon's entropy has been used in this study. Since AE entropy is obtained from the probability distribution of the discrete voltage value of each waveform, it is independent of threshold and other time dependent parameters. As such it is more effective than other traditional AE parameters in identifying the damage stages during the pullout process of straight steel fibers with different embedment lengths and aspect ratios.

## REFERENCES

[1] Pierre Richard and Marcel Cheyrezy. Composition of reactive powder concretes. *Cement and concrete research*, 25(7):1501–1511, 1995.

[2] MA Bajaber and IY Hakeem. Uhpc evolution, development, and utilization in construction: A review. *Journal of Materials Research and Technology*, 10:1058–1074, 2021.

[3] Murat Tuyan and Halit Yazıcı. Pull-out behavior of single steel fiber from sifcon matrix. *Construction and Building Materials*, 35:571–577, 2012.

[4] Rolf Breitenbücher, Günther Meschke, Fanbing Song, and Yijian Zhan. Experimental, analytical and numerical analysis of the pullout behaviour of steel fibres considering different fibre types, inclinations and concrete strengths. *Structural Concrete*, 15(2):126–135, 2014.

[5] Zemei Wu, Kamal Henri Khayat, and Caijun Shi. How do fiber shape and matrix composition affect fiber pullout behavior and flexural properties of uhpc? *Cement and Concrete Composites*, 90:193–201, 2018.

[6] Doo-Yeol Yoo, Junho Je, Hong-Joon Choi, and Piti Sukontasukkul. Influence of embedment length on the pullout behavior of steel fibers from ultra-high-performance concrete. *Materials Letters*, 276:128233, 2020.

[7] DT Kemp, P Bray, L Alexander, and AM Brown. Acoustic emission cochleography–practical aspects. *Scandinavian audiology. Supplementum*, 25:71–95, 1986.

[8] Farhan Tanvir Santo, Tariq Pervez Sattar, and Graham Edwards. Validation of acoustic emission waveform entropy as a damage identification feature. *Applied Sciences*, 9(19):4070, 2019.

[9] Nitin Burud and JM Chandra Kishen. Damage detection using wavelet entropy of acoustic emission waveforms in concrete under flexure. *Structural Health Monitoring*, 20(5):2461–2475, 2021.

[10] Ali Kahirdeh. *Energy dissipation and entropy generation during the fatigue degradation: Application to health monitoring of composites*. Louisiana State University and Agricultural & Mechanical College, 2014.

[11] Mehdi Amiri, Mohammad Modarres, and Enrique López Droguett. Ae entropy for detection of fatigue crack initiation and growth. In *2015 IEEE Conference on Prognostics and Health Management (PHM)*, pages 1–8. IEEE, 2015.

[12] Seyed Fouad Karimian, Mohammad Modarres, and Hugh A Bruck. A new method for detecting fatigue crack initiation in aluminum alloy using acoustic emission waveform information entropy. *Engineering fracture mechanics*, 223:106771, 2020.

[13] Ali Kahirdeh, Christine Sauerbrunn, and Mohammad Modarres. Acoustic emission entropy as a measure of damage in materials. In *AIP Conference Proceedings*, volume 1757. AIP Publishing, 2016.

[14] Claude E Shannon. A mathematical theory of communication. *The Bell system technical journal*, 27(3):379–423, 1948.